Tissue diagnosis using nanoscale morphological markers extracted from quantitative phase images

Masanori Takabayashi[a], Hassaan Majeed[b], Andre Kajdacsy-Balla[c], and Gabriel Popescu[b]

[a]Department of Systems Design and Informatics, Kyushu Institute of Technology, Iizuka, Fukuoka, Japan
[b]Beckman Institute of Advanced Science and Technology, University of Illinois at Urbana-Champaign, Urbana, IL, USA
[c]Department of Pathology, University of Illinois at Chicago, Chicago, IL, USA

ABSTRACT

The intrinsic markers of nanoscale morphological alteration in fixed tissue biopsy referred to as *disorder strength* and *local correlation length*, which can be easily and time-efficiently obtained from quantitative phase images, are introduced. After presenting how to extract these markers from quantitative phase images obtained by highly sensitive quantitative phase imaging system, spatial light interference microscopy (SLIM), we demonstrate the effectiveness of these markers for diagnosis of benign and malignant breast tissues.

Keywords: Quantitative phase imaging, Biopsy slide diagnosis, Breast cancer

1. INTRODUCTION

According to World Health Organization (WHO), cancer is the second leading cause of death globally.[1] About 9.6 million deaths by cancer in 2018 is estimated, and effective treatment strategies require early and accurate diagnosis of the disease. The gold standard method for cancer diagnosis is based on the microscopic investigation of a stained tissue biopsy by a clinical pathologist. The primary stain provides the necessary contrast needed for a trained pathologist to distinguish between normal and abnormal tissue morphology. However, this type of investigation is qualitative, depends on the details of tissue processing and, as a result, often leads to inter-observer variability. Thus, there is a need to provide an objective basis for evaluation based on physical metrics.

Quantitative phase imaging (QPI) is a label-free microscopy technique where contrast is generated by the optical path-length difference (OPD), which is the product of the local thickness and refractive index changes of the specimen.[2–4] For a thin specimen, such as a tissue histology, the thickness can be considered spatially invariant, in which case QPI images are proportional to a mean refractive index map, i.e., a refractive index map.[5–7] Since the refractive index is proportional to the dry mass content of cells and cellular matrix, it informs on tissue density as well as cell organization within tissue.[8,9] Tissue refractive index-based markers have been used in the past for medical diagnosis and prognosis of several types of cancers and diseases.[10–20] In addition to the advantages of label-free imaging, the contrast mechanism in QPI provides access to additional markers of disease, which are of value to histopathology. In particular, since QPI systems employ interferometric measurements, they are sensitive to subwavelength fluctuations in OPD in both space and time. Therefore, local fluctuations in quantitative phase images inform on nanoscale morphological alterations of cell structures, due to the dry mass accumulation as well changes in extracellular matrix components.

In this work, we introduce two types of intrinsic markers of nanoscale morphological alteration in fixed tissue biopsy referred to as *disorder strength* and *local correlation length*.[5,6] The disorder strength which is a marker of the local spatial fluctuations of refractive index was first used as a marker for pancreatic cancer diagnosis by Subramanian et al.[21] Their group used a spectroscopic imaging modality to measure this marker and have subsequently employed it in diagnostic studies related to prostate, colon, breast, lung, and other cancers.[21–29] Thereafter, Eldridge et al. successfully extracted the disorder strength from quantitative phase images and

---

demonstrated the relationship of the marker to cancer cell mechanical properties.[30] They applied this analysis to colon, skin, and lung cancer cells to demonstrate an inverse relationship between shear stiffness and disorder strength. Building on these results, Muñoz et al. used QPI to study the on-set and progression of shear stiffness changes during malignant transformation in bronchial epithelial cells.[31] Our group also showed that the disorder strength measured by spatial light interference microscopy (SLIM), a sensitive white light QPI method, is a quantitative marker of malignancy that can be used to classify benign and malignant breast tissue microarray (TMA) cores. On the other hand, the local correlation length is also a marker of the local spatial fluctuations of refractive index and have been proposed by our group. Although, the local correlation length map was computed by calculating the two-dimensional (2-D) correlation function over regions of an image leading to long computation times, we have proposed the efficient algorithm for calculating the local correlation length map, requiring a smaller number of calculation steps. We image the quantitative phase images of 20 benign, 16 grade 1, 16 grade 2, and 14 grade 3 malignant cores of breast TMA using SLIM, which is a high-sensitivity QPI method, able to detect sub-nanometer optical pathlength fluctuations. Then we classify these grades using the nanoscale marker(s): disorder strength, local correlation length and both of them.

2. QUANTITAIVE PHASE IMAGING (QPI)

QPI is a label-free microscopy technique where contrast is generated by the optical path-length difference, and the phase image, $\phi(x, y)$, measured in QPI is given by the equation:

$$\phi(x,y) \quad = \quad \frac{2\pi}{\lambda} \int_0^{L(x,y)} n(x,y,z)dz, \tag{1}$$

where $n(x, y, z)$ is the refractive index contrast between the tissue and the surrounding medium, $L(x, y)$ is the thickness of the tissue, and λ is the illumination wavelength. Here, in this work, we note that since we use tissue slices with constant thickness of 4 μm, the thickness can be rewritten as $L(x, y) \approx L$. Several methods have been proposed so far, however the figures of merit of QPI methods such as acquisition rate, temporal and spatial sensitivities and transverse resolution basically depend on the light source, interferometer and phase calculation algorithm used in the QPI method. We use spatial light interference microscopy (SLIM) which provides subwavelength sensitivity of OPD changes in both space and time.[2]

2.1 Spatial Light Interference Microscopy (SLIM)

A schematic of the SLIM setup is shown in Fig. 1(a). The SLIM module is attached to a commercial phase contrast microscope (PCM). The lamp filament is imaged onto the condenser annulus (Köhler illumination conditions), which is located at the front focal plane of the condenser lens. The specimen is located at the back focal plane of the condenser lens, and front focal plane of the objective. The scattered and unscattered fields are relayed by the objective and tube lenses. As a result, the expanded phase contrast image that has the intensity distribution in accordance with the phase contrast caused by the specimen is observed at the image plane. However, because the output of PCM is qualitative, the phase image, $\phi(x, y)$, cannot be directly retrieved from this image. The SLIM module extracts $\phi(x, y)$ by phase modulating the incident light with respect to the scattered light. The field at the image plane is Fourier transformed by the lens L1, such that the unscattered light can be spatially isolated from the scattered light. Since the incident light has the ring form, by displaying the corresponding ring pattern on the reflective liquid crystal phase modulator (LCPM), we ensure that the scattered light remains unaffected. Four phase shifts are applied to the unscattered light at increments of $\pi/2$ rad, as shown in Fig. 1(b). The corresponding four images captured by the charge coupled device (CCD) are obtained. Consequently, the quantitative phase image is retrieved as described in Ref.[2] The most important features of SLIM image is high sensitivities: according to previous work, sensitivities in OPD of 0.3 nm and 0.03 nm can be achieved in space and time, respectively.[2,4] Figure 1(c) shows the quantitative phase image and its expanded view of benign and malignant breast tissue samples. Since the thickness of tissue slice is constant, the quantitative information extracted from these images of refractive index changes can be used for diagnosis and prognosis of diseases.
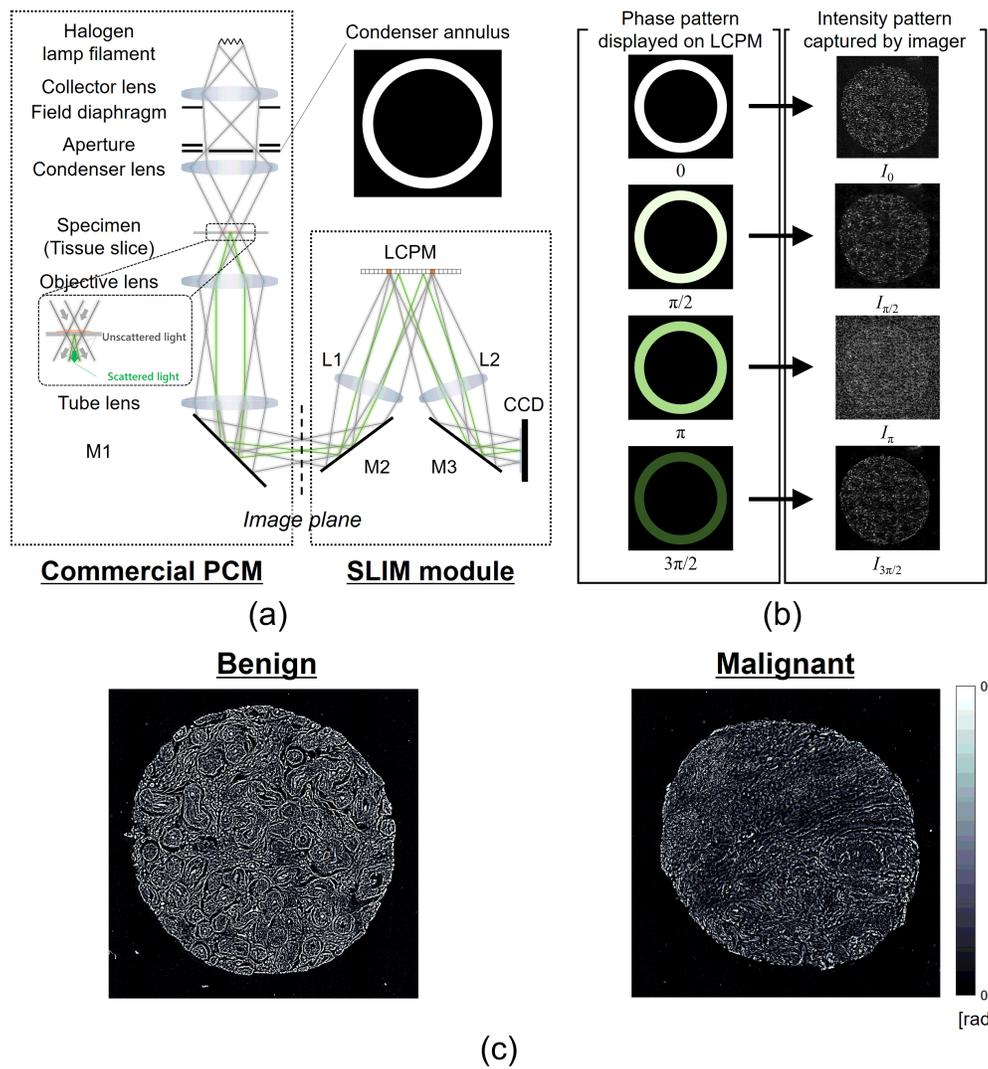
Figure 1. SLIM system. (a) Optical setup. (b) Phase patterns displayed on LCPM and corresponding intensity patterns captured by CCD. (c) Example of quantitative phase images of benign and malignant breast tissue cores.

2.2 Breast Tissue Microarrays

The samples comprised a TMA of cores constructed from breast tissue biopsies of 400 different patients. Each biopsy was formalin fixed and paraffin embedded before sectioning it into slices of 4-μm thickness each using a microtome. Two parallel, adjacent sections were selected from each biopsy, and one of these sections was stained using H & E, leaving the other one unstained. Cores were then constructed for both the stained and unstained tissue, and these were mounted on separate slides after deparaffinization, using xylene as the mounting medium. The stained samples were imaged using a bright-field microscope, and their images were used by a board-certified pathologist for diagnosing each core. In this paper, we studied benign tissue as well as cancerous tissue from three different grades: benign ($N = 20$), malignant (grade 1, $N = 16$), malignant (grade 2, $N = 16$), and malignant (grade 3, $N = 14$). Each patient consented to their tissue samples being used as part of the study, and the process of obtaining consent was approved by the Institute Review Board (IRB Protocol Number 2010-0519) at University of Illinois at Chicago (UIC). The data analysis was conducted on the samples at the University of Illinois at Urbana–Champaign (UIUC) after all patient identifiers had been removed. The procedures used in this study for conducting experiments using human subjects were also approved by the institute review board at UIUC (IRB Protocol Number 13900).

3. NANOSCALE MORPHOLOGICAL ALTERATION MARKERS

3.1 Disorder Strength

By definition, the disorder strength map, $L_d(x, y)$, is expressed as:

$$L_d(x,y) \quad = \quad < \Delta n(x,y)^2 >_w l_c, \tag{2}$$

Here, $< \cdots >_w$ denotes the average within the window of interest, Δ means the difference from its average, i.e., $\Delta n(x,y) = n(x,y) - < n(x,y) >_w$, and l_c is the spatial autocorrelation length. Figure 2(a) shows the quantitative phase image $\phi(x,y)$, which contains information about the spatial variation of the refractive index change of tissues as expressed by Eq. 1. The local variance and average of the phase has the form, respectively,

$$< \Delta\phi(x,y)^2 >_w \quad = \quad \left(\frac{2\pi L}{\lambda}\right)^2 < \Delta n(x,y)^2 >_w, \tag{3}$$

and

$$< \phi(x,y) >_w^2 \quad = \quad \left(\frac{2\pi L}{\lambda}\right)^2 n_{mean}^2, \tag{4}$$

Here, nmean is the average of the refractive index in the tissue. Thus, the local refractive index fluctuation map, which is independent of the thickness, can be computed as

$$< \Delta n(x,y)^2 >_w \quad = \quad \frac{< \Delta\phi(x,y)^2 >_w}{< \phi(x,y) >_w^2} n_{mean}^2. \tag{5}$$

Therefore, we can rewrite Eq. 2 and obtain the final form to calculate the disorder strength map from the quantitative phase image as

$$L_d(x,y) \quad = \quad \frac{< \Delta\phi(x,y)^2 >_w}{< \phi(x,y) >_w^2} n_{mean}^2 l_c. \tag{6}$$

In our calculation, we used a window of 5 × 5 pixels (0.125 μ m/pixel). Figure 2(b) shows the map of $< \Delta\phi(x,y)^2 >_w / < \phi(x,y) >_w^2$. Since our interest is the fluctuation only in the tissue region, the background pixels were excluded as shown in Fig. 2(c). Consequently, the disorder strength can be calculated using the resulting phase image by mutiplying the constant refractive index, n_{mean} of 1.38 and the mean spatial autocorrelation length of all tissues, l_c.
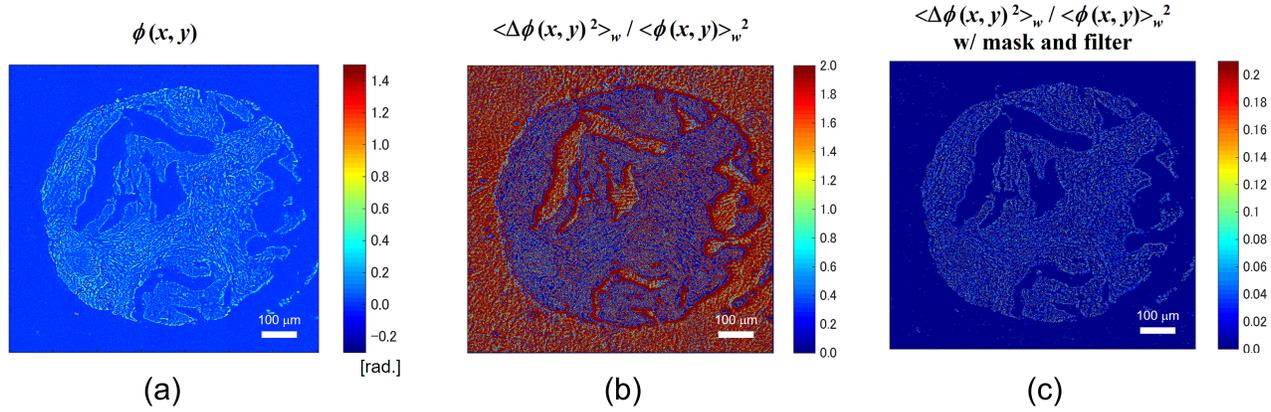
Figure 2. Calculation procedure of DS map. (a) Quantitaitve phase image. (b) Phase fluctuation map. (c) Phase fluctuation map after filtering and masking to exclude undesired pixels.

3.2 Local Correlation Length

The local correlation length depends on the morphological disorder, i.e., local refractive index fluctuations. When the refractive index is spatially disordered, the spatial autocorrelation length within the local area will shorten. In general, the spatial autocorrelation length is calculated as the width of the spatial autocorrelation function. According to the Wiener-Khinchin theorem, the 2D spatial autocorrelation function can be obtained by taking inverse 2D Fourier transform of the spatial power spectrum. In other words, two 2D Fourier transforms for each image, leading to long computation times. Thus, to avoid this problem, we propose a new procedure that performs these calculation in the frequency-domain.

First, as shown in Fig.3, we define the local correlation function as

$$\Gamma(x, y; x', y') = t(x, y; x', y') \otimes_{x,y} t(x, y; x', y'), \tag{7}$$

where $\otimes_{x,y}$ denotes the 2D correlation operation over (x, y). Function $t(x, y; x', y')$ is a local phase function centered at (x', y') and is expressed as

$$t(x, y; x', y') = \phi(x, y)w(x, y; x', y') - <\phi(x, y)w(x, y; x', y')>_{(x,y)}, \tag{8}$$

where $w(x, y; x', y') = \mathrm{rect}\left(\frac{x-x'}{a}\right)\mathrm{rect}\left(\frac{y-y'}{a}\right)$ is a local window function centered at (x', y'), of width of a. The angular brackets denote averaging within the local window.

Next, we define the local correlation length map, $\rho(x', y')$, as the variance of the probability density which can be obtained by normalizing $\Gamma(x, y; x', y')$ by $\iint \Gamma(x, y; x', y')dxdy$:

$$\rho^2(x', y') = \frac{\iint (x^2 + y^2)\Gamma(x, y; x', y')dxdy}{\iint \Gamma(x, y; x', y')dxdy}. \tag{9}$$

Here, $\rho(x', y')$ can be related to the bandwidth map of the spatial power-spectrum, $\tau(x', y')$, as $\rho(x', y')\tau(x', y') = 2\pi$. The local bandwidth, $\tau(x', y')$, itself is defined as

$$\tau^2(x', y') = \frac{\iint (k_x^2 + k_y^2)|t(k_x, k_y; x', y')|^2 dk_x dk_y}{\iint |t(k_x, k_y; x', y')|^2 dk_x dk_y}. \tag{10}$$

where $t(k_x, k_y; x', y')$ is the Fourier transform of $t(x, y; x', y')$ along (x, y). Using the differentiation property of Fourier transforms as well as Parseval＇s theorem, this equation can be rewritten as

$$\tau^2(x', y') = \frac{\iint \left[|\frac{\partial}{\partial x} t(x, y; x', y')|^2 + |\frac{\partial}{\partial y} t(x, y; x', y')|^2 \right] dxdy}{\iint |t(x, y; x', y')|^2 dxdy}, \tag{11}$$
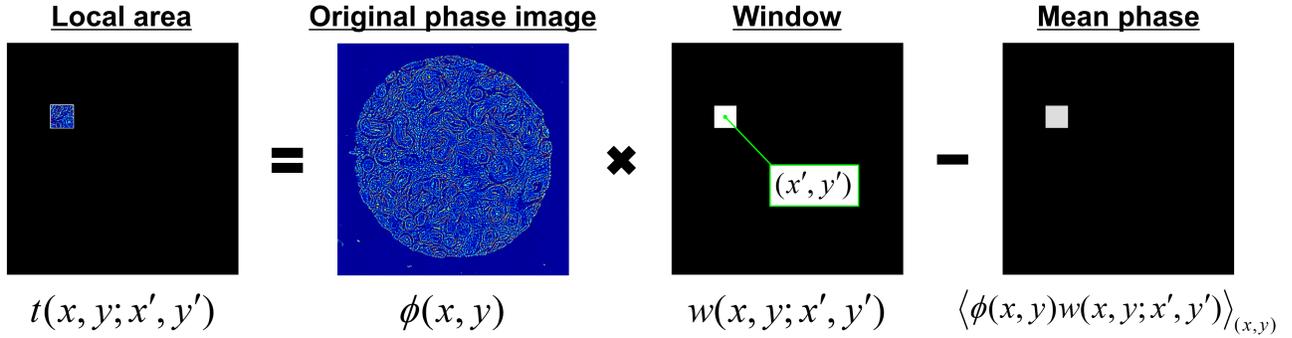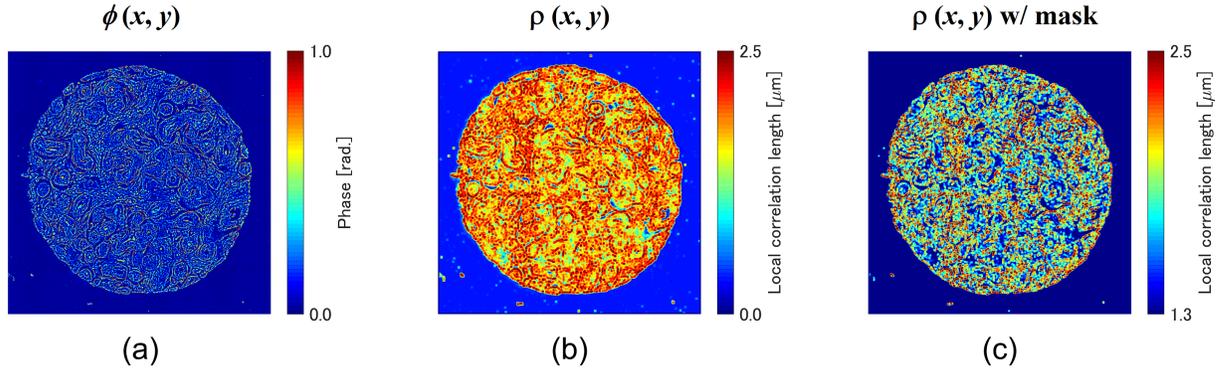
Figure 3. Definition of $t(x, y; x', y')$.

Figure 4. Calculation procedure of local correlation length map. (a) Quantitaitve phase image. (b) Local correlation length map. (c) Local correlation length map after masking to exclude undesired pixels.

Finally, we can obtain the final result as

$$\rho(x', y') \quad = \quad 2\pi \sqrt{\frac{\iint |t(x, y; x', y')|^2 \, dxdy}{\iint \left[|\frac{\partial}{\partial x} t(x, y; x', y')|^2 + |\frac{\partial}{\partial y} t(x, y; x', y')|^2\right] dxdy}}. \tag{12}$$

Using Eq. 12, the local correlation length maps can be calculated as shown in Fig.4 which were obtained from the quantitative phase image.

4. BREAST CANCER CLASSIFICATION USING NANOSCALE MARKER

Figure 5 compares the average of $\mathbb{L}_d(x, y)$ between benign and malignant cores (grade 1, 2 and 3). To extract only tissue regions, the pixels which satisfy $< \phi(x, y) >_w < 0.075$ rad. and $< \Delta\phi(x, y)^2 >_w / < \phi(x, y) >_w^2 > 2.7$ were excluded. The p-values which were obtained by two-sided Wilcoxon ranksum test are listed in the row named p-value (DS) in Table 1. Although the statistically significant differences are indicated between benign and malignant cores, the results show that the inter-grade cores are hardly distiguished. On the other hand, Fig. 6 compares the average divided by the standard deviation of ρ map between benign and malignant cores (grade 1, 2 and 3). We can use any feature quantity of ρ map, however the average divided by the standard deviation was adopted because it indicated the best p-value. To extract only tissue regions, the background pixels were segmented out by setting a threshold in the $\rho(x, y)$ map. This threshold value was determined empirically, and all pixels having correlation lengths below 1.3 μm were treated as background. The p-values which were obtained by two-sided Wilcoxon ranksum test are listed in the row named p-value (LCL) in Table 1. Since the p-value between 20 benign and 46 malignant cores was 0.000876, the local correlation length correlates with
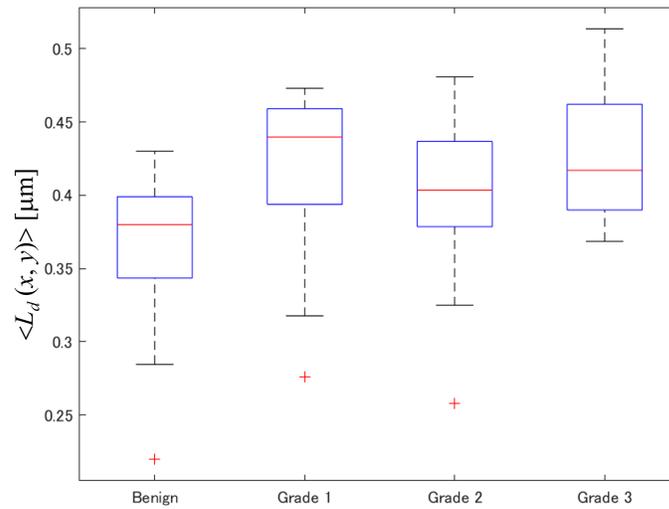
Figure 5. Disorder strength of benign ($N = 20$) and grade 1 ($N = 16$), grade 2 ($N = 16$), and grade 3 ($N = 14$) tissues.
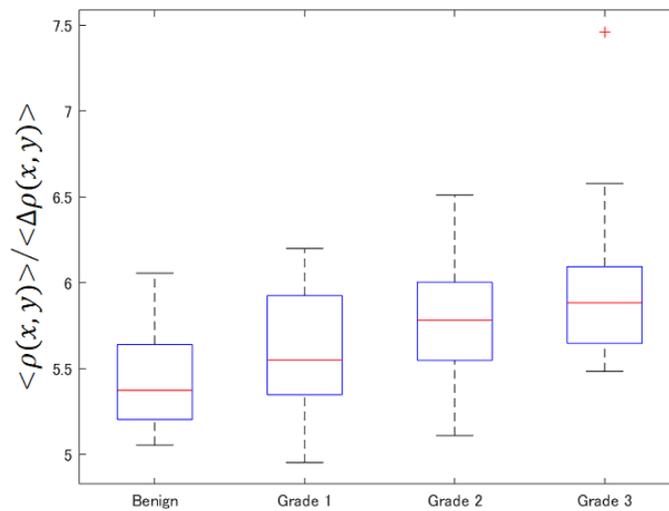

Figure 6. Local spatial autocorrelation length of benign ($N = 20$) and grade 1 ($N = 16$), grade 2 ($N = 16$), and grade 3 ($N = 14$) tissues.

cancer grades. Furthermore, the results indicate that the statistically significant differences between cores with more than 2 inter-grade differences. However, it may need to be combined with other markers for more detail separation of grades. We conclude that the local correlation map can potentially be used by clinical pathologists as a supplementary label-free disease marker for gauging the onset of malignancy especially in borderline cases. The results of classification using both disorder strength and local correlation length will be presented at the conference.

Table 1. The p-values between different grades

Grades to be evaluated	p-value (DS)	p-value (LCL)
Benign - Malignant (G1, G2, G3)	0.000833	0.000876
Benign and Malignant (G1) - Malignant (G2, G3)	0.136913	0.000335
Benign - Malignant (G1)	0.002914	0.101101
Benign - Malignant (G2)	0.040033	0.005891
Benign - Malignant (G3)	0.004849	0.000498
Malignant (G1) - Malignant (G2)	0.299994	0.193509
Malignant (G1) - Malignant (G3)	0.950279	0.018837
Malignant (G2) - Malignant (G3)	0.371447	0.417581

5. CONCLUSIONS AND FUTURE WORKS

We have introduced two types of cancer markers of nanoscale morphological alteration referred to as *disorder strength* and *local correlation length* and demonstrated classification of breast cancer tissues. Although neighboring grades were not distingished, the effectiveness of these markers to classify more than two grades including benign and malignant tissues was shown. We need to consider tissue diagnosis using plural markers and machine learning based classification to achieve distinguishing between neighboring grades. The improved results of classification accuracy by using both disorder strength and local correlation length will be presented at the conference.

ACKNOWLEDGMENTS

REFERENCES

[1] "Fact sheet: Cancer." https://www.who.int/news-room/fact-sheets/detail/cancer. (Accessed: 25 September 2019).

[2] Popescu, G., [*Quantitative Phase Imaging of Cells and Tissues*], McGraw Hill (2011).

[3] Popescu, G., "The power of imaging with phase, not power," **70**(5), 34–40 (2017).

[4] Wang, Z., Millet, L., Mir, M., Ding, H., Unarunotai, S., Rogers, J., Gillette, M. U., and Popescu, G., "Spatial light interference microscopy (slim)," *Optics Express* **19**, 1016–1026 (2011).

[5] Takabayashi, M., Majeed, H., Kajdacsy-Balla, A., and Popescu, G., "Disorder strength measured by quantitative phase imaging as intrinsic cancer marker in fixed tissue biopsies," *PLoS ONE* **13**(3), 1–10 (2018).

[6] Takabayashi, M., Majeed, H., Kajdacsy-Balla, A., and Popescu, G., "Tissue spatial correlation as cancer marker," *Journal of Biomedical Optics* **24**, 6 (2019).

[7] Kandel, M. E., Sridharan, S., Liang, J., Luo, Z., Han, K., Macias, V., Shah, A., Patel, R., Tangella, K., Kajdacsy-Balla, A., Guzman, G., and Popescu, G., "Label-free tissue scanner for colorectal cancer screening," *Journal of Biomedical Optics* **22**(6), 66016 (2017).

[8] Mir, M., Wang, Z., Shen, Z., Bednarz, M., Bashir, R., Golding, I., Prasanth, S. G., and Popescu, G., "Optical measurement of cycle-dependent cell growth," *Proc. Natl. Acad. Sci. USA* **108**(32), 13124–9 (2011).

[9] Cooper, K. L., Oh, S., Sung, Y., Dasari, R. R., Kirschner, M. W., and Tabin, C. J., "Multiple phases of chondrocyte enlargement underlie differences in skeletal proportions," *Nature* **495**(7441), 375–8 (2013).

[10] Majeed, H., Nguyen, T. H., Kandel, M. E., Kajdacsy-Balla, A., and Popescu, G., "Label-free quantitative evaluation of breast tissue using spatial light interference microscopy (slim)," *Scientific Reports* **8**(1), 6875 (2018).

[11] Majeed, H., Sridharan, S., Mir, M., Ma, L., Min, E., Jung, W., and Popescu, G., "Quantitative phase imaging for medical diagnosis," *J Biophotonics* **10**(2), 177–205 (2017).

[12] Majeed, H., Okoro, C., Kajdacsy-Balla, A., Toussaint, K. C., J., and Popescu, G., "Quantifying collagen fiber orientation in breast cancer using quantitative phase imaging," *Journal of Biomedical Optics* **22**(4), 46004 (2017).

[13] Majeed, H., Kandel, M. E., Han, K., Luo, Z., Macias, V., Tangella, K., Balla, A., and Popescu, G., "Breast cancer diagnosis using spatial light interference microscopy," *Journal of Biomedical Optics* **20**(11), 111210 (2015).

[14] Nguyen, T. H., Sridharan, S., Macias, V., Kajdacsy-Balla, A., Melamed, J., Do, M. N., and Popescu, G., "Automatic gleason grading of prostate cancer using quantitative phase imaging and machine learning," *Journal of Biomedical Optics* **22**(3), 36015 (2017).

[15] Park, Y., Best, C. A., Badizadegan, K., Dasari, R. R., Feld, M. S., Kuriabova, T., Henle, M. L., Levine, A. J., and Popescu, G., "Measurement of red blood cell mechanics during morphological changes," *Proc. Natl. Acad. Sci. USA* **107**(15), 6731–6 (2010).

[16] Sridharan, S., Macias, V., Tangella, K., Kajdacsy-Balla, A., and Popescu, G., "Prediction of prostate cancer recurrence using quantitative phase imaging," *Scientific Report* **5**, 9976 (2015).

[17] Wang, Z., Tangella, K., Balla, A., and Popescu, G., "Tissue refractive index as marker of disease," *Journal of Biomedical Optics* **16**(11), 116017 (2011).

[18] Wang, P., Bista, R., Rohit, B., Brand, E., R., and Liu, Y., "Spatial-domain low-coherence quantitative phase microscopy for cancer diagnosis ," *Optics Letters* **35**(17), 2840 (2010).

[19] Pham, H. V., Pantanowitz, L., and Liu, Y., "Quantitative phase imaging to improve the diagnostic accuracy of urine cytology," *Cancer cytopathology* **124**(9) (2016).

[20] Bista, R. K., Wang, P., Bhargava, R., Uttam, S., Hartman, D. J., Brand, R. E., and Liu, Y., "Nuclear nano-morphology markers of histologically normal cells detect the "field effect" of breast cancer," *Breast Cancer Res Treat* **135**(1), 115–24 (2012).

[21] Subramanian, H., Pradhan, P., Liu, Y., Capoglu, I. R., Rogers, J. D., Roy, H. K., Brand, R. E., and V., B., "Partial-wave microscopic spectroscopy detects subwavelength refractive index fluctuations: an application to cancer diagnosis," *Optics Letters* **34** (2009).

[22] Chandler, J. E., Subramanian, H., Maneval, C. D., White, C. A., M.D., R. M. L., and Backman, V., "High-speed spectral nanocytology for early cancer screening," *Journal of Biomedical Optics* **18**(11), 1–10, 10 (2013).

[23] Damania, D., Roy, H. K., Subramanian, H., Weinberg, D. S., Rex, D. K., Goldberg, M. J., Muldoon, J., Cherkezyan, L., Zhu, Y., Bianchi, L. K., Shah, D., Pradhan, P., Borkar, M., Lynch, H., and Backman, V., "Nanocytology of rectal colonocytes to assess risk of colon cancer based on field cancerization," *Cancer Research* **72**(11), 2720 (2012).

[24] Damania, D., Subramanian, H., Tiwari, A. K., Stypula, Y., Kunte, D., Pradhan, P., Roy, H. K., and Backman, V., "Role of cytoskeleton in controlling the disorder strength of cellular nanoscale architecture," *Biophysical Journal* **99**(3), 989–996 (2010).

[25] Konda, V. J. A., Cherkezyan, L., Subramanian, H., Wroblewski, K., Damania, D., Becker, V., Gonzalez, M. H. R., Koons, A., Goldberg, M., Ferguson, M. K., Waxman, I., Roy, H. K., and Backman, V., "Nanoscale markers of esophageal field carcinogenesis: potential implications for esophageal cancer screening," *Endoscopy* **45**(12), 983–988 (2013).

[26] Roy, H. K., Brendler, C. B., Subramanian, H., Zhang, D., Maneval, C., Chandler, J., Bowen, L., Kaul, K. L., Helfand, B. T., Wang, C.-H., Quinn, M., Petkewicz, J., Paterakos, M., and Backman, V., "Nanocytological field carcinogenesis detection to mitigate overdiagnosis of prostate cancer: A proof of concept study," *PLOS ONE* **10**(2), e0115999 (2015).

[27] Roy, H. K., Damania, D. P., DelaCruz, M., Kunte, D. P., Subramanian, H., Crawford, S. E., Tiwari, A. K., Wali, R. K., and Backman, V., "Nano-architectural alterations in mucus layer fecal colonocytes in field carcinogenesis: Potential for screening," *Cancer Prevention Research* **6**(10), 1111 (2013).

[28] Roy, H. K., Subramanian, H., Damania, D., Hensing, T. A., Rom, W. N., Pass, H. I., Ray, D., Rogers, J. D., Bogojevic, A., Shah, M., Kuzniar, T., Pradhan, P., and Backman, V., "Optical detection of buccal epithelial nanoarchitectural alterations in patients harboring lung cancer: Implications for screening," *Cancer Research* **70**(20), 7748 (2010).

[29] Stypula-Cyrus, Y., Damania, D., Kunte, D. P., Cruz, M. D., Subramanian, H., Roy, H. K., and Backman, V., "Hdac up-regulation in early colon field carcinogenesis is involved in cell tumorigenicity through regulation of chromatin structure," *PLOS ONE* **8**(5), e64600 (2013).

[30] Eldridge, W. J., Steelman, Z. A., Loomis, B., and Wax, A., "Optical phase measurements of disorder strength link microstructure to cell stiffness," *Biophysical Journal* **112**(4), 692–702 (2017).

[31] Muñoz, A., Eldridge, W. J., Jakobsen, N. M., Sørensen, H., Wax, A., and Costa, M., "Cellular shear stiffness reflects progression of arsenic-induced transformation during g1," *Carcinogenesis* **39**(2), 109–117 (2017).